Optical Engineering 48(10), 104301 (October 2009)

Applications of spectral analysis and filter design in laser frequency locking for Na Doppler lidars

John A. Smith
Xinzhao Chu
Wentao Huang
Bo Tan
University of Colorado at Boulder
Cooperative Institute for Research in Environmental Sciences
and
Department of Aerospace Engineering Sciences
216 UCB
Boulder, Colorado 80309
E-mail: Xinzhao.Chu@Colorado.edu

Abstract. A dye ring laser is stabilized to a D_{2a} Doppler-free feature of sodium vapor using a LabVIEW®-based, phase-sensitive servo. Locking precision and stability, at better than ±1 MHz, are suitable for Na lidar applications. This performance was achieved with improved digital filtering and new approaches to the problem. The inverse (type II) Chebyshev discrete filter employed demonstrates superior filtering and computational efficiency plus improved flexibility. New approaches include the determination of optimum modulation frequency, laser-tuning sensitivity, and bandwidth requirements via spectral analyses of the noise spectrum, derivative scan, and modulated spectrum. This practice guides a user in selecting the system operation parameters and negotiating the trade-offs involved when expanding the filter's passband. Allan deviation plots provide a quantitative description of the short- and long-term frequency excursions. A comparison of Allan deviation plots before and after locking shows a substantial improvement in stability throughout time scales from 0.10 to 10 s. [DOI: 10.1117/1.3251080]

Subject terms: wavelength modulation; LabVIEW; dye ring laser; Na lidar; saturation-absorption spectroscopy; filter design; spectral analysis; frequency stabilization.

Paper 090146R received Feb. 28, 2009; revised manuscript received Aug. 5, 2009; accepted for publication Sep. 3, 2009; published online Oct. 20, 2009.

1 Introduction

Sodium resonance fluorescence Doppler lidars, the current "golden standard" of fluorescence lidars, have been instrumental to advancing knowledge of thermal, dynamical, and chemical structures of the mesosphere and lower thermosphere.[1,2] Narrowband Na Doppler lidars rely on a continuous wave (CW) laser to seed desired spectral properties on transmitted pulses, such as a specific center frequency and narrow linewidth. Both dye ring lasers[1,2] and optically mixed neodymium-doped yttrium aluminum garnet (Nd:YAG) lasers[3] are in usage today to fulfill this purpose. These lasers are locked to a D_{2a} Doppler-free feature of Na vapor[2,4,5] to provide a predictable and stable frequency standard for the lidar system, enabling precision wind and temperature measurements. Long-term accuracy, precision, and stability of within 1 MHz are demanded in the seed laser frequency. A software-based direct-intensity comparison technique has been applied to lock dye ring lasers in Na lidar.[1,2] A drawback to this method is the susceptibility to background light and laser-intensity fluctuations, resulting in low locking precision and stability. Systems have been demonstrated that lock CW lasers more reliably to an absorption feature using wavelength modulation[6] in conjunction with digital processing techniques.[7,8] Our previous work,[9] a phase-sensitive servo loop emulated in National Instruments LabVIEW®, successfully demonstrated a system of diode laser stabilization with wavelength modulation and digital processing. However, the dye jet and long cavity used in dye ring lasers are more susceptible to acoustic and mechanical vibrations than diode lasers, resulting in substantial noise throughout the available tuning bandwidth. Therefore, dye ring lasers present a unique challenge to these locking systems. The Colorado State University lidar group was able to achieve an absolute stability of a few megahertz by using a setup that modulates the high-speed correction element, overriding the control box's own locking circuitry.[10] This method involves additional hardware, such as a dedicated lock-in amplifier, and detailed knowledge of the laser's control electronics.

We have addressed these issues by introducing several advancements to the system presented in our previous work.[9] A unique filtering architecture—borrowed from telecommunications[11]—and a proportional-integral-derivative (PID) servo loop enable this simple system to achieve better than ±1 MHz of precision and stability in 1-h trials by working alongside the laser's existing locking electronics. In addition, we present systematic approaches to the problem, such as determining the required servo bandwidth and setting an optimal modulation rate and laser tuning sensitivity. The laser locking system was developed and tested on a Coherent 899-21 dye ring laser system tuned to the Na absorption at 589 nm, but the system and approaches can be applied to any laser and spectroscopic system. In the following, we introduce the methodology and then present performance results. Conclusions and proposed future improvements are also provided.

0091-3286/2009/$25.00

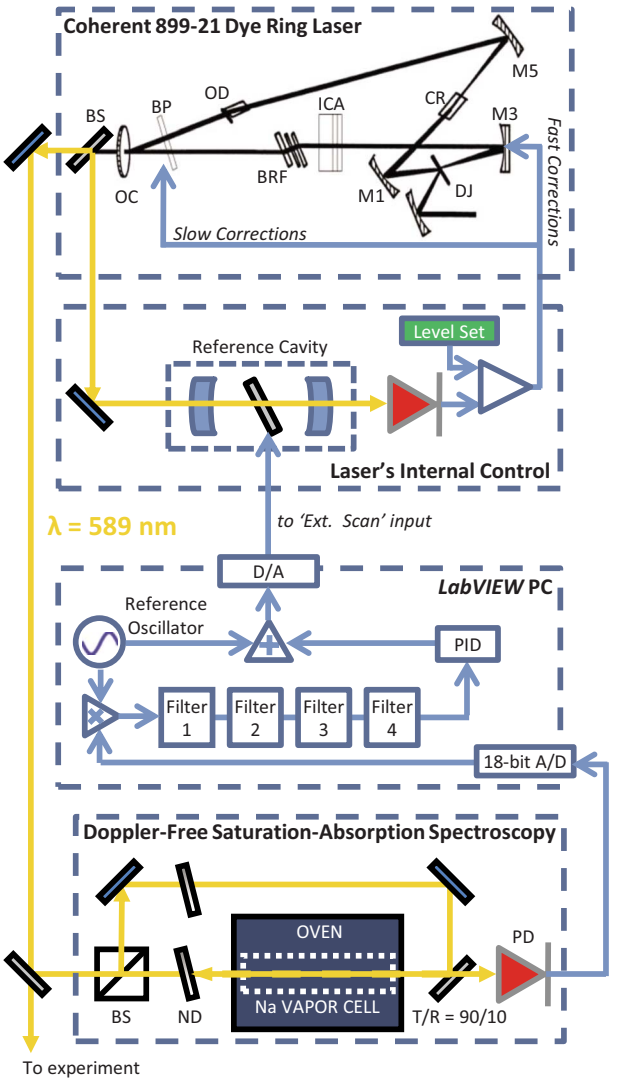

Fig. 1 Dye ring laser control, spectroscopic, and locking feedback system showing overlapping, counterpropagating pump, and probe beams for Doppler-free spectroscopy; filters 1–4 are the inverse Chebyshev low-pass, 30-Hz notch, 60-Hz notch, and 960-Hz second harmonic notch filters, respectively. In the Coherent 899-21 dye ring laser subdiagram (taken from Refs. 12 and 13), OC: output coupler of the laser cavity, BP: Brewster plate supplying slow locking corrections, BRF: Birefringence filter, ICA: Intracavity assembly consisting of thin and thick etalons, CR: Compensation rhomb, DJ: Dye jet, OD: Optical diode, M3: PZT-driven mirror of the laser cavity supplying fast locking corrections, M1 and M5: two other mirrors of the laser cavity. On the LabVIEW PC subdiagram, multiplication and filters 1–4 (low pass) accomplish lock-in amplification. Blue arrows indicate signal connections. Our A/D-D/A converter is a National Instruments PCI-6281 with 18-bit input resolution. (Color online only.)

2 Methods

The laser and control systems are illustrated in Fig. 1. Our saturation-absorption spectroscopy setup is similar to those used in Refs. 5 and 9, but with some modifications. An extra beamsplitter (with a transmission/reflection ratio of 90/10%) allows pump and probe beams to overlap completely, reducing the necessary pump laser power. Doppler-free features in this setup experience less power broadening, providing more distinct Doppler-free saturation-absorption features and the best absolute frequency discrimination possible (Fig. 2). Our laser, a Coherent 899-21 dye ring (shown in the top portion of Fig. 1), possesses a piezoelectric transducer (PZT) element and a Brewster plate that together adjust the optical length of the cavity. This combination provides both high- and low-speed corrections to the output laser frequency with the normalized transmission of a reference cavity providing frequency discrimination.[12,13] Because the Coherent 899-21 dye ring laser's internal correction elements derive their discriminant signals from this cavity, which has no absolute frequency reference, the dye ring laser exhibits poor long-term frequency stability. On smaller time scales of ~1 s, however, a stability of ~1 MHz can be expected (Fig. 3).

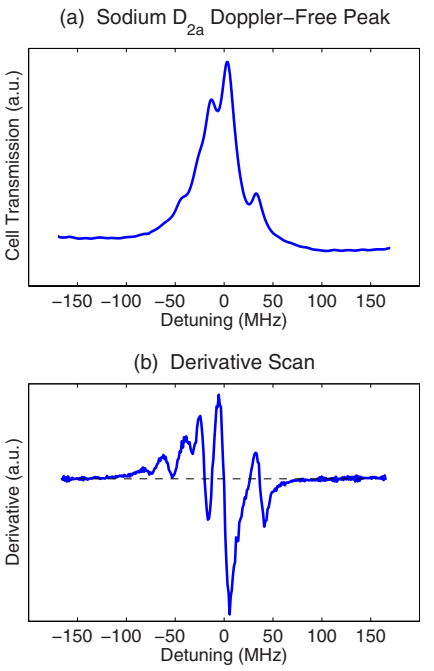

Fig. 2 (a) Recorded Doppler-free spectrum at the Na D_{2a} absorption line and (b) the derivative signal obtained from wavelength modulation.

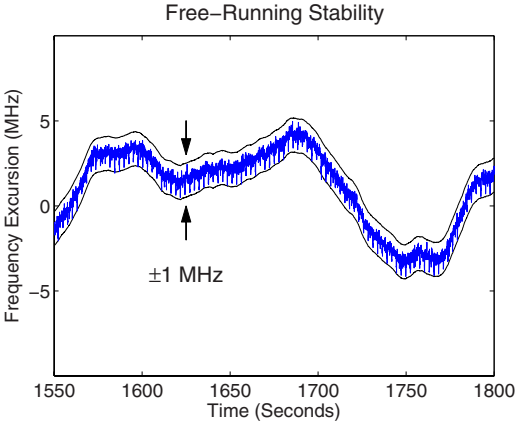

Fig. 3 Time series of wavelength meter-recorded frequency excursions from the mean showing the free-running stability of the dye ring laser; the laser control box was set to "lock" (internal servos engaged).

Our system complements the laser's existing servos by effectively locking the reference cavity to a Na vapor Doppler-free absorption line and allowing the laser to follow. For this locking, a Brewster galvo inside the reference cavity is modulated via the "Ext. Scan" input by a LabVIEW-generated modulation signal. Because the reference cavity is mostly disturbed by slow processes, such as ambient temperature and pressure fluctuations, only drift corrections are required. As a result, only a low modulation frequency is required, which mechanical tuning elements can handle. Note that the external feedback system is similar to that in Ref. 9, with the photodiode-detected transmission signal multiplied in a point-by-point fashion by the reference modulation, then low-pass filtered to derive an error signal for the PID servo.

A detailed treatment of wavelength-modulation spectroscopy and lock-in amplification used in our servo system is provided in our previous work.[9] Here, we briefly outline the basic concepts and the internal control of the dye ring laser to make the method presentation clear. On the side of a Na absorption feature, a small oscillation of laser frequency will produce a cell transmission that oscillates at the same frequency, a so-called 1-f signal. On the opposite side of the absorption feature, this 1-f signal is the same frequency but 180 deg out of phase. Taylor expansion would reveal higher-order components, but these components are considered noise in this study. At the very peak of the absorption feature, the cell transmission produces an apparent doubling of the oscillation, a "2-f" response and the 1-f signal disappears. We extract the amplitude of the 1-f by mixing it with the original reference modulation, resulting in a dc term proportional to the 1-f signal's amplitude and noise shifted to higher frequencies. A low-pass filter isolates the dc term, removing most $1/f$ noise and harmonics, but also necessarily limiting the servo bandwidth because the filter's passband is finite. Locking-in to the 1-f signal therefore produces an error signal that is positive on one side of the absorption, negative on the other, and zero at the very peak of the absorption.[9] The PID block computes an appropriate correction voltage from the error signal by summing the magnitude, time integral, and time derivative of the error signal with appropriate gains applied to each component. Correction voltages are passed to the galvo drive, in turn changing the reference cavity length and its peak transmission frequency. The laser frequency is then forced by its own servo loop (Fig. 1) to follow the reference cavity. This servo loop uses an internal error signal derived from fringe-side detection of the reference cavity. Part of the internal error signal is applied to the cavity's PZT-driven mirror (M3 in Fig. 1) to correct for fast cavity length variations. The other part is used to drive the rotating Brewster plate to compensate for slower cavity length changes. By locking the reference cavity and allowing the laser to follow, the laser's center frequency is kept to the Na Doppler-free peak.

2.1 *Determination of Servo Loop Bandwidth Requirement*

The central frequency of any given laser system will exhibit a drift rate that depends on the observational time scale. In order for this locking system to be effective, its response bandwidth must be greater than the drift bandwidth. However, increasing the response bandwidth entails widening the low-pass filter's passband, which could permit significant noise. It is instructive to place an upper bound on the drift bandwidth so as to limit the passband as much as possible. A technique we employed to estimate the drift bandwidth is described below.

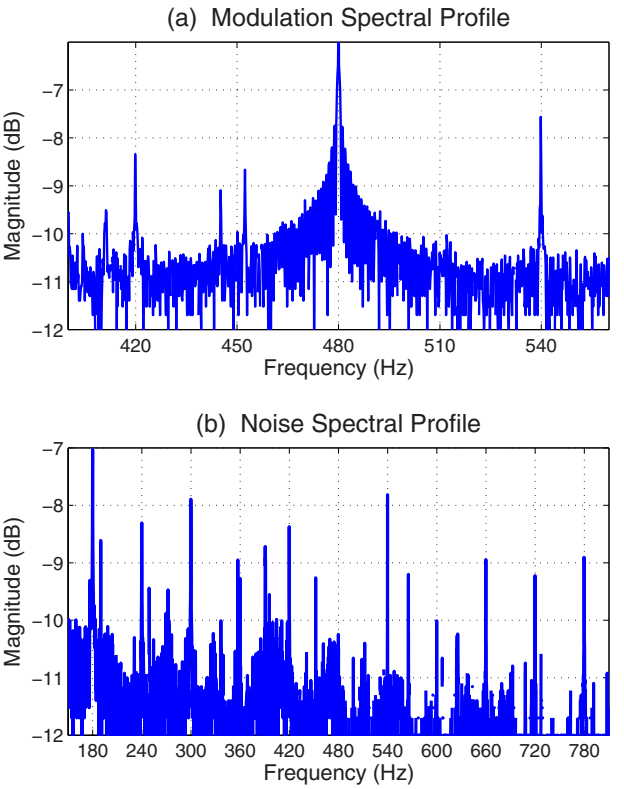

Fig. 4 Autocorrelated Fourier spectrum for the modulation spectral profile showing the (a) degree of spectral broadening and (b) noise spectral profile centered about the 480-Hz modulation frequency. Note the 60-Hz harmonics and noise components about 450 Hz (a). Also note the extensive noise throughout and the 60-Hz harmonics (b). These results may not be universal, but may serve as an example.

A 1-f return signal results from adding a modulation to the side of an absorption, the amplitude of which depends on the local derivative of the absorption about the oscillation's center. If the oscillation center is perturbed by random disturbances, then the 1-f amplitude will change correspondingly and produce an apparent broadening of the 1-f modulation spectrum as shown in Fig. 4(a). We oscillate the laser where the local second derivative is maximized and sample the photodiode-detected vapor cell transmission at a high rate, then compute a power spectrum. Here, we attempt to rigorously show that the power spectral density of the 1-f return signal provides information about the laser's drift bandwidth. We start by approximating the spectral shape of transmitted intensity $I_T(\omega)$ about the center of oscillation by series expansion. This is valid as long as the depth of modulation is much smaller than the width of the spectral feature in question. Defining ω_0 as the laser's central frequency, $\omega_D(t)$ as the time-dependent ran-

dom disturbance to ω_0, $\delta\omega$ as the modulation amplitude, and Ω as the modulation frequency, we get Eq. (1), where prime denotes derivation with respect to ω

$$\omega = \omega_0 + \omega_D(t) + \Delta\omega \sin(\Omega t),$$
$$I_T[\omega_0 + \omega_D(t) + \Delta\omega \sin(\Omega t)] \approx I_T[\omega_0 + \omega_D(t)] + I_T'[\omega_0 + \omega_D(t)]\Delta\omega \sin(\Omega t). \quad (1)$$

Because the random disturbances are very small compared to the width of the Na absorption spectral feature, we may further linearize the series expansion about ω_0 as in

$$I_T[\omega_0 + \omega_D(t) + \Delta\omega \sin(\Omega t)] \sim I_T[\omega_0 + \omega_D(t)] + [I_T'(\omega_0) + I_T''(\omega_0)\omega_D(t)]\Delta\omega \sin(\Omega t). \quad (2)$$

The first term on the right-hand side of Eq. (2) is a linear function of disturbance $\omega_D(t)$ at zero frequency, and the second term is another linear function of that disturbance but shifted in Fourier space by the Ω modulation. The zero-frequency region is dominated by $1/f$ noise; thus, we disregard its contribution to the complete Fourier transform. This assumption is valid because it is known *a priori* that the spectral distribution of ω_D is much smaller than Ω, making these two terms easily distinguishable spectrally. The region about Ω has a relatively small and flat spectral noise profile. Invoking the convolution theorem and replacing functions of ω_0 and their derivatives with constants, we write the time domain return signal in frequency domain as in Eq. (3) using FT to denote Fourier transform. Constants α and β denote the first and second derivatives, respectively, of $I_T(\omega_0)$ with respect to ω

$$\begin{aligned}\mathrm{FT}\{[\alpha + \beta \cdot \omega_D(t)]\sin(\Omega t)\} &= \mathrm{FT}\{\alpha + \beta \cdot \omega_D(t)\} \otimes \mathrm{FT}\{\sin(\Omega t)\} \\ &= \mathrm{FT}\{\alpha\} \otimes \mathrm{FT}\{\sin(\Omega t)\} + \mathrm{FT}\{\beta \cdot \omega_D(t)\} \otimes \mathrm{FT}\{\sin(\Omega t)\}. \end{aligned} \quad (3)$$

The constant offset α will not affect the degree of spectral broadening, nor will the scaling factor β. Therefore, we ignore the first term in Eq. (3) and group the scaling factor in the second to produce Eq. (4), introducing ω' as the Fourier-space frequency variable and $A(\omega)$ as the random disturbance spectrum.

$$\begin{aligned}\mathrm{FT}\{I_T[\omega_0 + \omega_D(t) + \Delta\omega \sin(\Omega t)]\} &\sim \mathrm{FT}\{\omega_D(t)\} \otimes \mathrm{FT}\{\sin(\Omega t)\} \\ &= A(\omega') \otimes \delta(\omega' - \Omega) = A(\omega' - \Omega). \end{aligned} \quad (4)$$

The final result is the spectrum of random disturbances about the modulation center, causing a broadening effect as shown in Fig. 4(a). The modulation's pedestal is symmetric about the center of modulation and extends from the center to where it becomes indistinguishable from background noise; this definition of full broadening gives an estimate of 60–80 Hz, the drift bandwidth being one-half this amount. Note that we have ignored certain frequency disturbances, such as laser line-shape width and technical noise. These sources of uncertainty are grouped into background noise, because our sampling rates were well below their Nyquist criterion. In summary, we now have an estimate for the required low-pass filter's passband width.

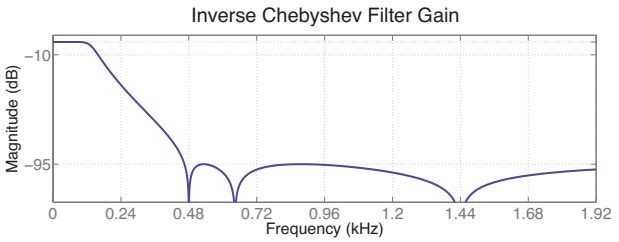

Fig. 5 An inverse Chebyshev filter with 95-dB stopband attenuation and 120-Hz passband implemented in the phase sensitive servo loop; note the stopband nulls at 1-*f* (480-Hz) and 3-*f* (1440-Hz) harmonics; cutoff and sampling frequencies are 465 and 5750 Hz, respectively.

2.2 *Optimal Modulation Rate and Filtering Considerations*

Lock-in detection works by shifting a signal in frequency from a region of high spectral noise to a region of low spectral noise, as explained previously. Typically, a user would accomplish this by modulating the signal as fast as possible. The dye ring laser tuning element, however, is limited to the sub-800-Hz range, and there is substantial noise throughout this range [Fig. 4(b)] with most noise concentrated at 60-Hz harmonics. A modulation rate of 480 Hz was chosen because the surrounding region is relatively clean and it is also the only reachable frequency where there are no 60-Hz harmonics. The 480-Hz region is flanked on either side by the 540 and 420-Hz noise harmonics, and there exists a set of noise components at 450 Hz. After heterodyning these noise terms with the 480-Hz modulation, the sum frequencies can be ignored because they will be far beyond the passband and the difference terms become 60 Hz for both adjacent harmonics. The noise terms previously at 450 Hz become 30 Hz. As a result, three neighboring noise sources can be efficiently removed with just two low-Q notch filters at 60 and 30 Hz, reducing both the group delay and computational demand of the filter cluster. By selectively removing these noise sources, the filter passband criterion derived in Sec. 2.1 is now satisfied.

In our previous system,[9] an elliptic filter was employed because it possessed a null in the stopband that could be positioned over the first harmonic in the heterodyned signal. A disadvantage was the inherent loss of signal due to passband ripple and the difficulty of positioning stopband nulls over additional harmonics. Also, the filter parameters could not be adjusted to accommodate wider or narrower passbands without affecting stopband null positions, thus making the filter highly inflexible. Another possibility was the boxcar average[8] which effectively removes all harmonics, but this architecture again lacks an adjustable passband. An inverse Chebyshev filter was implemented instead.[11] The sixth-order variant possesses a sharp roll-off as a consequence of its three stopband nulls, the first and third of which can be positioned independently over the first and third harmonics (Fig. 5) by adjusting the cutoff and sam-

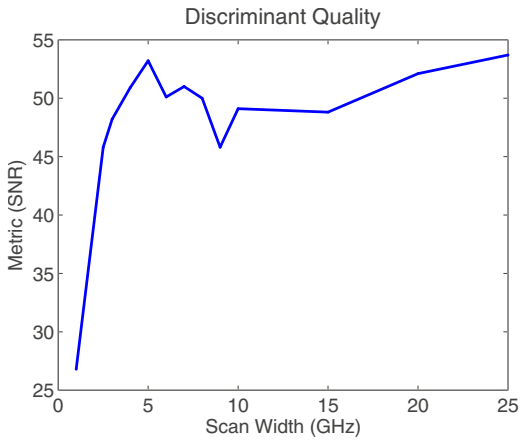

Fig. 6 A plot of the discriminant SNR versus scan width; modulation amplitude and scanning ramp voltages were scaled to compensate for the changing scan width in order to isolate the dye-ring-laser control box as a source of noise.

pling frequencies. A notch filter removes the second harmonic. Additionally, the stopband attenuation can be adjusted freely to widen or narrow the passband without significantly affecting the positions of the stopband nulls. Tight control of the passband is critical to our application since significant noise exists throughout the range of tuning frequencies.

2.3 *Laser Control Settings*

The Coherent 899-21 laser control box has a setting for "Scan Width," which controls the available range of frequencies that users can scan when applying a ±5-V ramp voltage to the "Ext. Scan" input. The scan width can be set between 10 MHz and 29.99 GHz, 10 MHz being the setting that makes the laser least sensitive to detuning. In Smith et al.,[9] we found that reducing the sensitivity of the external cavity diode laser by removing the 10× gain at the PZT tuning input created the best locking conditions. With lower sensitivity the laser is less susceptible to unintentional detuning from line noise. Several tests were run on the dye ring laser control box to see which scan-width setting provided the best signal-to-noise ratio (SNR) in the derivative scan plotted in Fig. 2(b), defined as the ratio of the peak value to the background standard deviation. Close analysis showed an optimal SNR at a scan width of 5 GHz with a steep degradation in SNR below 5 GHz (Fig. 6), likely a result of noise introduced by regulation from control box electronics. Findings may vary between laser systems. We choose 5 GHz as our scan-width setting.

3 Results

All trials were recorded on a HighFinesse WSU-2 wavelength meter with 1-ms exposure time. This wavelength meter combines six Fizeau interferometers and fringe counting algorithms to achieve precision of <1 MHz. The USB transfer rate from wavemeter to PC was ~40 Hz. A stability of within ±1 MHz was achieved in hour-long trials recorded on the wavelength meter (Fig. 7). Allan variance is another measure of stability,[14] one that is recommended by the IEEE for frequency standards, especially with regard to the long-term walk-off issue.[15] Allan deviation plots were computed using a provided MATLAB script[16] to measure the stability across multiple time scales. A substantial improvement was observed across all available time scales, from 0.10 to 10 s (Fig. 8). The small deviations at large timescales imply that drift is completely removed. An illustration of the frequency drift reflected by the Allan deviation is provided in Figure 9.

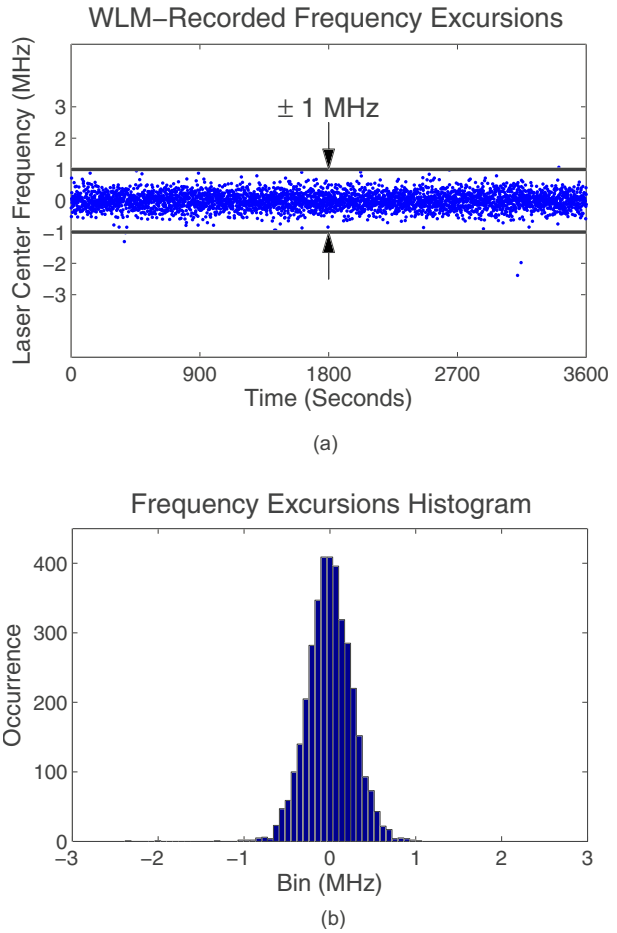

Fig. 7 (a) Excursions from the center frequency recorded at 1-s intervals and (b) a histogram generated from the same data. Wavelength meter temperature drift was removed by subtracting a 20-s sliding/boxcar average.

With the wavelength meter's 1-ms averaging time, disturbance introduced by the 480-Hz reference modulation may not be represented accurately. We use a 2-f analysis technique introduced in Ref. 9 to determine the amplitude of disturbances resulting from the induced modulation (Fig. 10). A model of the absorption line shape is constructed based on physical considerations, and the apparent doubling of the modulation (1-f) about the peak is modeled and compared to experimental data. Analysis of the photodiode-detected transmission on an oscilloscope revealed a 2-f peak-to-peak amplitude of <1 mV, implying a 1-f modulation amplitude of <1 MHz (Fig. 10). The line shape used would be broader than the actual line shape because it is an average over several scans; therefore, it should only be considered as placing an upper bound on the modulation amplitude.

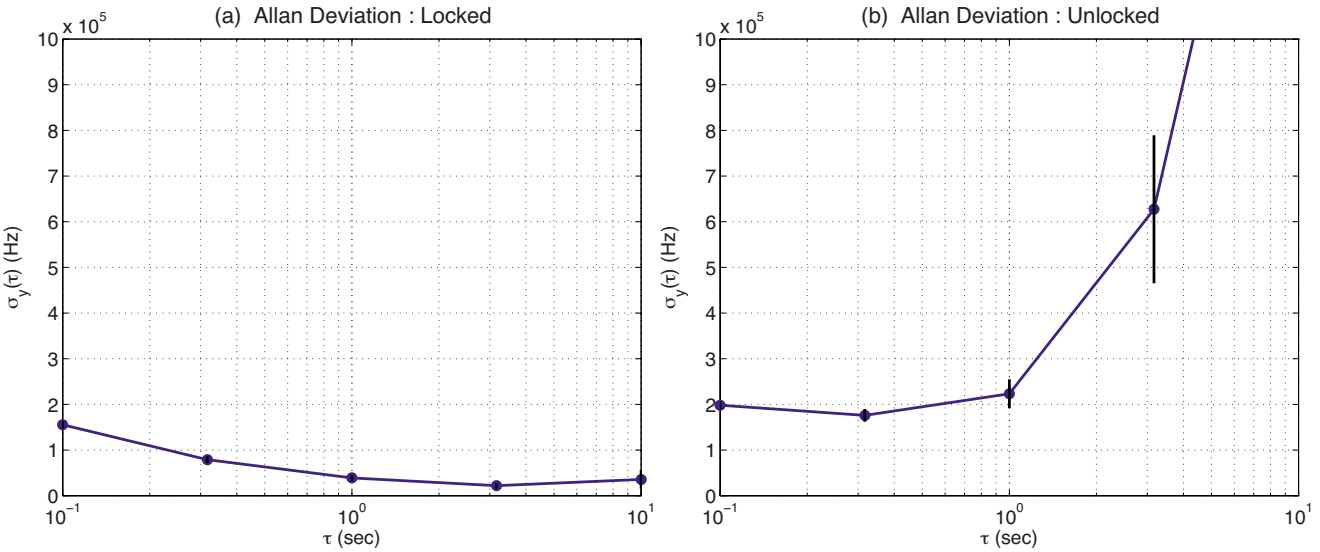

Fig. 8 Allan deviations (N=2000) of the (a) locked and (b) unlocked dye ring laser with laser frequency sampled at 19.3 Hz. There are increasing deviations at the longer time scales as a result of laser drift in the unlocked case; drift is completely removed in the locked case though, as expected.

4 Conclusions

We have demonstrated a simple wavelength-modulation-based locking system capable of reliably and conveniently locking dye ring lasers with both long and short-term stability of well within 1 MHz, suitable for Na Doppler lidar applications. These results are achieved via a systematic approach to the problem and an improved digital filtering technique. We apply a noise spectral analysis to determine an optimum modulation frequency that is suitable for mechanical tuning elements and produces the least posthomodyned noise. Analysis of the derivative scan helps us to determine the best laser-tuning sensitivity (i.e., scan width in the case of the dye ring laser) that results in the highest SNR in the discriminant signal. A modulation spectrum technique is employed to determine the drift rate of the laser central frequency from the apparent broadening, thus placing a quantitative requirement on the passband of the filters used in the phase-sensitive detection. An inverse Chebyshev filter is an efficient design that, properly configured, can accomplish both the low-pass filtering and notching out of harmonics. This filter also possesses a highly adjustable passband for comprise between filter delay and discriminant SNR. Allan variance shows substantial improvement of the laser stability in time scales from

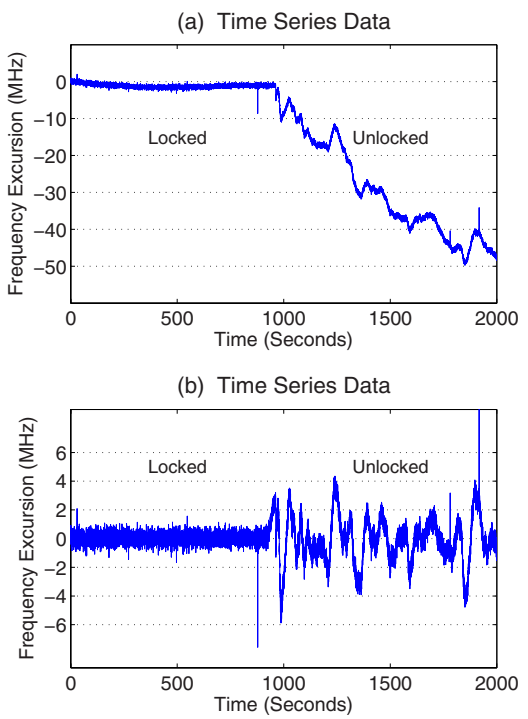

Fig. 9 Wavelength meter-recorded, (a) contiguous frequency time series data and (b) the same data with a 100-s sliding average subtracted; the dye ring laser's internal servos were engaged throughout the trial.

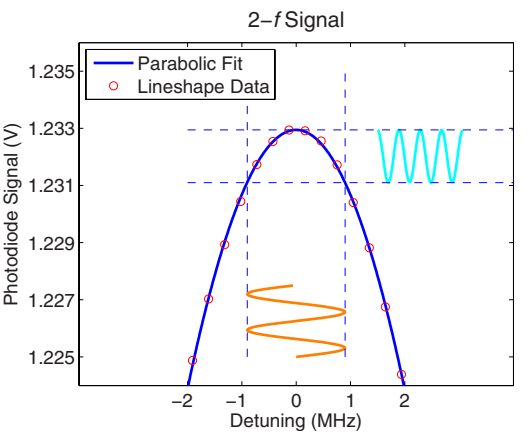

Fig. 10 A graphic showing the Doppler-free Na D_{2a} absorption peak with a modulation added to model the 2-f response signal; note that this places an upper bound of ~1 MHz on the modulation's amplitude.

0.10 to 10 s. Further wavelength meter measurements and the 2-f analysis prove the laser locking precision and stability to be within ± 1 MHz. Our procedure demonstrated above is general; however, the specifics are examples and may not be universal for all systems. The spectral properties of environmental noise may vary. Analysis should be performed on an individual basis to determine optimal modulation frequency, required passband width, etc. A future improvement is to determine a systematic way of picking the PID gains, which has the potential to enhance performance substantially. A transfer function characterizing the tuning element would be required, which is the largest obstacle to creating a simulation of the feedback.

Acknowledgments

We sincerely acknowledge Johannes Wiig and Archie Brown for constructing a reliable sodium vapor cell and oven assembly. This project is an effort by the Consortium Technology Center, operating under the umbrella of the Consortium of Resonance and Rayleigh Lidars (CRRL). Code is available on request. Work was supported by National Science Foundation Grants No. ATM-0545353 (CRRL), No. ATM-0645584 (CAREER), and No. ATM-0723229 (MRI).

References

1. X. Chu and G. Papen, "Resonance fluorescence lidar for measurements of the middle and upper atmosphere," in *Laser Remote Sensing*, T. Fujii and T. Fukuchi, Eds., pp. 179–432, CRC Press, Boca Raton (2005).
2. C. Y. She, J. R. Yu, H. Latifi, and R. E. Bills, "High-spectral-resolution fluorescence light detection and ranging for mesospheric sodium temperature measurements," *Appl. Opt.* **31**, 2095–2106 (1992).
3. T. Kawahara, S. Nozawa, R. Fujii, N. Saito, S. Wada, K. Akagawa, Y. Saito, F. kobayashi, A. Nomura, J. Yue, and C. Y. She, "A high power sodium temperature lidar based on injection seeded LD-pumped Nd:YAG lasers," in *Proc. of 24th Int. Laser Radar Conf. (ILRC)*, Boulder, CO, June 23–27, 2008, pp. 861–864 (2008).
4. W. Demtröder, *Laser Spectroscopy*, 3rd ed., Springer, New York (2003).
5. X. Chu, W. Huang, J. S. Friedman, and A. T. Brown, "CRRL/CTC: Doppler-free saturation-absorption and polarization spectroscopy for resonance fluorescence Doppler lidars," in *Proc. of 24th Int. Laser Radar Conf. (ILRC)*, Boulder, CO, June 23–27, 2008, pp. 809–812 (2008).
6. J. Supplee, E. Whittaker, and W. Length, "Theoretical description of frequency modulation and wavelength modulation spectroscopy," *Appl. Opt.* **33**, 6294–6302 (1994).
7. L. Dong, W. Yin, W. Ma, and S. Jia, "A novel control system for automatically locking a diode laser frequency to a selected gas absorption line," *Meas. Sci. Technol.* **18**, 1447–1452 (2007).
8. T. Ahola, J. Hu, and E. Ikonen, "A digital control system for the iodine stabilized He-Ne laser," *Rev. Sci. Instrum.* **69**, 1934–1937 (1998).
9. J. Smith, X. Chu, W. Huang, J. Wiig, and A. Brown, "LabVIEW-based laser frequency stabilization system with phase-sensitive detection servo loop for Doppler LIDAR applications," *Opt. Eng.* **47**(11), 114201 (2008).
10. M. White, "A frequency-agile Na Lidar for the measurement of temperature and velocity in the mesopause region," PhD dissertation, Colorado State University, pp. 32–36, 1999.
11. K. Shenoi, *Digital Signal Processing in Telecommunications*, Prentice Hall, Englewood Cliffs, NJ (1995).
12. "Coherent 899 Tunable Lasers," Training Course Lecture, 1998.
13. Coherent 899-21 Dye Ring Laser, Operator's Manual, 1990.
14. D. W. Allan, "Statistics of atomic frequency standards," *Proc. IEEE*, **54**(2), 221–230 (1966).
15. D. W. Allan, N. Ashby, and C. C. Hodge, "The science of timekeeping," Hewlett-Packard (HP) Application Note No. 1289, pp. 56–65 (1997).
16. W. J. Riley, "Addendum to a test suite for the calculation of time domain frequency stability," *Proc. of 1996 IEEE Freq. Control Symp.*, pp. 880–882, IEEE, New York (1996).

John A. Smith received his BS in engineering physics from the Colorado School of Mines in 2006 and MS in aerospace engineering sciences from the University of Colorado at Boulder (UCB) in 2009. He is now continuing toward his PhD under a NASA Earth and Space Science Fellowship. His research focuses on advancements in lidar instrumentation and applications therein.

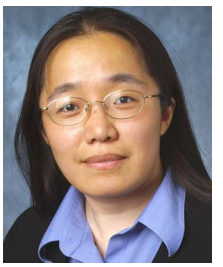

Xinzhao Chu is currently an associate professor in the Department of Aerospace Engineering Sciences, UCB. She is a fellow of the Cooperative Institute for Research in Environmental Sciences (CIRES). She received her BS and PhD in physics and electrical engineering from Peking University in 1991 and 1996, respectively. During her tenure at the University of Illinois at Urbana-Champaign from 1997 to 2005, she made the first pole-to-pole lidar measurements of the middle and upper atmosphere in 1999 to 2001. She published "Resonance fluorescence lidar for measurements of the middle and upper atmosphere," in *Laser Remote Sensing*[1] in 2005. Now She teaches a graduate-level lidar course at UCB and serves as the director of Consortium Technology Center for the national Consortium of Resonance and Rayleigh Lidars. Dr. Chu is the principle investigator for the National Science Foundation Major Research Instrumentation mobile Fe-resonance/Rayleigh/Mie Doppler lidar.

Wentao Huang is currently a research scientist in the CIRES, at UCB. He received his BS and PhD in physics and optics in the field of nonlinear optics and ultrafast time-resolved spectroscopy from Peking University, Beijing, China, in 1998 and 2003, respectively. Afterward he worked as a postdoctoral research associate in physical chemistry in the Department of Chemistry, University of Illinois at Urbana-Champaign. He joined CIRES in 2006 and has been working on innovative lidar technology, laser spectroscopy, and atmospheric science since then.

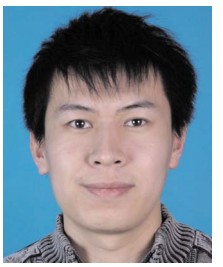

Bo Tan received his BS in space physics from Peking University in 2006. He is now a PhD student in the Department of Aerospace Engineering Sciences at UCB, working in the CIRES. His research focuses on using lidar wind and temperature retrievals to study the thermal and dynamic structures of the mesosphere and lower thermosphere, including tides and gravity waves. He is also interested in using various atmospheric models, together with satellite and lidar data, to study the atmosphere.